Composite Structures 176 (2017) 748–756

Contents lists available at ScienceDirect

Composite Structures

journal homepage: www.elsevier.com/locate/compstruct

Flexural performance evaluation of NSM basalt FRP-strengthened concrete beams using digital image correlation system

Sherif M. Daghash, Osman E. Ozbulut *

Department of Civil and Environmental Engineering, University of Virginia, P.O. Box 400742, Charlottesville, VA 22904-1000, United States

ARTICLE INFO

Article history:
Received 16 February 2017
Revised 18 April 2017
Accepted 7 June 2017
Available online 9 June 2017

Keywords:
Near-surface-mounted
BFRP
DIC technique
Concrete structures strengthening

ABSTRACT

This study investigates the flexural behavior of reinforced concrete beams strengthened with near surface mounted (NSM) basalt fiber reinforced polymer (BFRP) bars. A total of five concrete beams with a length of 2100 mm were prepared with different internal longitudinal reinforcement and strengthening reinforcement ratios. Four-point bending tests were conducted under monotonic loading. A digital image correlation (DIC) technique was used to monitor full-field displacement and strain contours as well as mid-span deflections. The strains in the BFRP bars were recorded using strain gauges. The force-displacement curves, longitudinal strains in NSM reinforcement, and crack widths were computed and used to evaluate the performance of the strengthened beams. Results indicate that the NSM BFRP bars can successfully restore the original capacity of a concrete beam with a corroded internal reinforcement while providing a more ductile behavior. In addition, the ultimate load capacity of the reinforced concrete beams can be augmented using NSM BFRP bars but in an expense of smaller deflection capacity.

© 2017 Elsevier Ltd. All rights reserved.

1. Introduction

Over their service life, concrete structures experience deterioration due to various factor such as increased service loads, environmental effects, and poor design or quality of construction [1]. Replacement of all aging and structurally deficient structures may require significant resources and time. Strengthening can be a more economical and sustainable alternative to extend the intended lifespans of concrete structures. Fiber reinforced polymer (FRP) composites have been widely used to strengthen concrete structures due to their favorable properties such as high corrosion resistance, lightweight and high tensile strength [2,3]. In particular, near surface mounted (NSM) FRP strengthening systems have been considered as an effective technique in restoring strength of concrete structures [4–7]. In NSM strengthening, reinforcing bars or strips are inserted into longitudinal grooves that are cut in concrete cover of strengthened structure and bonded to the structure using either epoxy adhesives or cement mortars. NSM strengthening method can offer several advantages compared to externally bonded (EB) strengthening systems, where sheets of fiber reinforced polymers (FRPs) are bonded to external surface of concrete. In particular, NSM strengthening avoids the premature debonding and rupture failure usually experienced in EB systems and protects the strengthening reinforcement from environmental effects and external impacts. It also requires limited surface preparation, minimal installation time, and enables strengthening in the negative moment regions of structural elements [8–10].

A large number of researchers have investigated the bond behavior of NSM FRP reinforcement considering the effects of different parameters such as groove size, adhesive material, surface texture, and bonded length [11,12]. A few researchers have comparatively studied the bond efficiency of EB and NSM FRP strengthening systems [13,14]. Seo et al. [13] found that the NSM systems have bond strength 1.5 times higher than the EB systems. Bilotta et al. [14] also reported that the NSM technique delayed the debonding compared to EB systems. They also indicated that the tensile strength of the FRP materials is better exploited in NSM systems, resulting in much higher utilization factors.

In most of the previous research on NSM flexural strengthening of concrete beams, carbon FRP (CFRP) strips or bars have been used as the reinforcement [15–17]. It was found that the beams strengthened with CFRP NSM reinforcement can significantly increase yielding and ultimate load capacity. However, CFRP NSM strengthened beams mostly exhibited a brittle failure mode. Several researchers have investigated the use of glass FRP (GFRP) in NSM applications. Sharaky et al. [18] strengthened reinforced concrete (RC) beam specimens with a clear span of 2400 mm using NSM CFRP or GFRP bars and tested under four-point bending

* Corresponding author.
E-mail addresses: smd7an@virginia.edu (S.M. Daghash), ozbulut@virginia.edu (O.E. Ozbulut).

http://dx.doi.org/10.1016/j.compstruct.2017.06.021
0263-8223/© 2017 Elsevier Ltd. All rights reserved.

loading. Compared to the reference beam, there were 55% and 66% increases in the ultimate load capacity of the CFRP-strengthened beams when one and two NSM CFRP bars were used, respectively. The increases in the ultimate load capacities of the GFRP-strengthened beams were 41% and 59% for the beams strengthened with one and two GFRP bars, respectively. However, the deflections of the CFRP-strengthened beams at ultimate load was almost half of those of GFRP-strengthened beams, indicating more brittle behavior. In a more recent study, El-Gamal et al. [19] also investigated the flexural behavior of NSM glass and carbon FRP strengthened beams. They reported that the NSM CFRP strengthened beams shows much more brittle behavior but reaches higher ultimate load capacities compared to NSM GFRP strengthened beams.

Basalt fibers are a class of the environmentally-friendly inorganic natural fibers that have been recently used in FRP industry to fabricate basalt-epoxy composites [20]. Basalt fibers have high resistance to alkalinity in surrounding concrete, excellent resistance to aggressive environmental conditions, high chemical stability and great fatigue resistance [21]. Basalt FRP (BFRP) composites have recently emerged as an alternative and advantageous FRP type that can be used in civil engineering applications [22–24]. BFRPs exhibits lower ultimate strength and modulus of elasticity than CFRPs but have significantly lower costs and wider working temperature ranges. Compared to GFRPs, they have somewhat higher mechanical properties, better chemical stability and similar or lower cost. However, the studies on the use of BFRP bars in NSM strengthening of concrete structures have been limited. Zhu et al. [25] studied the fire resistance of the RC beams strengthened with BFRP bars and Gopinath et al. [26] focused on the bond behavior of the BFRP bars for the NSM strengthening applications. A detailed study on the flexural performance of NSM BFRP strengthened beams is missing.

Digital image correlation (DIC) technique is a non-contact optical-numerical measuring system. It can provide full-field measurements of displacements and strains based on comparison among sequential images of the region of interest (ROI) captured by digital cameras at different levels of loading [27]. Therefore, DIC technique is preferred over traditional methods of measurement such as LVDTs and strain gauges, which require direct contact with the specimen surface and provide only pointwise measurements. Additionally, traditional gauges can be damaged or separated from the specimen at high levels of deformation. As a result, DIC technique was used in various applications in concrete structures, including crack detection and behavior analysis of full-scale reinforced and prestressed concrete elements [28,29], analyzing fracture properties of concrete-concrete and FRP-concrete interfaces [30,31], and structural health monitoring of bridges [32].

This study explores the use of BFRP bars as NSM reinforcement to strengthen RC beams in flexure. A total of five concrete beams were prepared with different internal longitudinal reinforcement and strengthening reinforcement ratios and tested under monotonic four-point bending loading. The DIC system was used to monitor the full-field displacement and strain contours and mid-span deflections. The development of major flexural crack was also monitored and analyzed in each beam specimen. The performance of BFRP bars in NSM strengthening of RC beams was assessed in terms of force and displacement capacities at various loading stages, longitudinal strains in NSM reinforcement, and crack widths in the concrete.

2. Experimental program

2.1. Materials

The BFRP bars used in this study are commercially labeled as GATORBAR™ and were supplied by Neuvokas, Inc. The bars had nominal diameter of 9.5 mm with fiber content of 80% by weight. The average tensile strength and modulus of elasticity of the BFRP bars were 1109.5 MPa, and 44.3 GPa, respectively, and the average strain at peak stress was 3.21%, as provided by the manufacturer. Fig. 1 shows typical stress-strain curve for the BFRP bars used in this study under uniaxial tension.

Ribbed steel bars were used as the longitudinal and transverse reinforcement. The yield strength, ultimate strength, and modulus of elasticity of steel bars were 413.7 MPa, 517.1 MPa and 200 GPa, respectively. The steel bars with 12 mm diameter were used as the tension reinforcement, while the bars with 10 mm diameter were used as stirrups and top reinforcement. The beams were cast using ready-mixed concrete. Five standard cylinders with dimensions of 150 × 300 mm were prepared for the compression testing. The average compressive strength of the concrete cylinders after 28 days was 38 MPa. Sikadur® 32 Hi-modulus epoxy adhesive was used to bond the BFRP bars to the concrete beams. The tensile strength of the epoxy was 48 MPa according to the manufacturer.

2.2. Design of RC beams

A total of five concrete beams were fabricated and tested. As shown in Fig. 2(a), the beams had a total length of 2100 mm and clear span of 1950 mm. All the beams had a rectangular cross section of 150 × 300 mm. Fig. 2(b) shows the cross section detailing of the tested beams. The first specimen was the reference beam (REF or S3B0), which had three steel bars as the main reinforcement and no strengthening BFRP bars. Two specimens had three longitudinal steel bars and strengthened with either one (S3B1) or two (S3B2) BFRP bars. Two other specimens were designed to have two longitudinal steel bars and again strengthened with either one (S2B1) or two (S2B2) BFRP bars.

The RC beams with two or three steel reinforcing bars had longitudinal reinforcement ratio of 0.66% and 1.0%, respectively, and the beam sections were under-reinforced. For all the beams, the stirrups were spaced at 125 mm to ensure flexural failure of the beams. In the strengthened beams, foam was placed inside the formwork before casting of concrete to form the grooves. The grooves had cross section of 25 × 25 mm and length of 1800 mm. After hardening of concrete, the foam was removed and surfaces of grooves were cleaned. The epoxy was then used to fill half of the groove's depth and the 1800 mm-long strengthening bars were placed inside the grooves and lightly pressed. The grooves were completely filled with epoxy, and the bottom surface of the beams was leveled. The epoxy cured for 7 days before testing the beams.

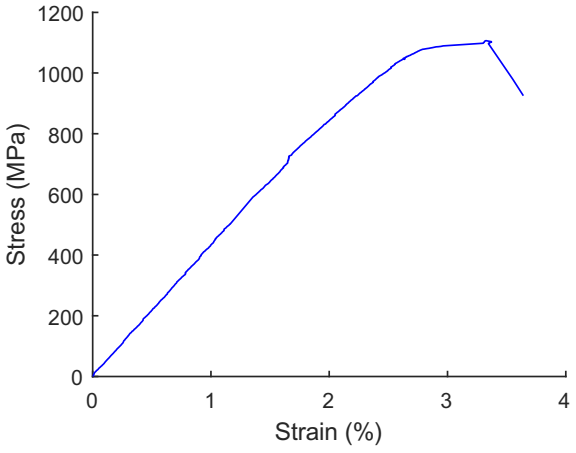

Fig. 1. Stress-strain curve of BFRP bar tested in uniaxial tension.

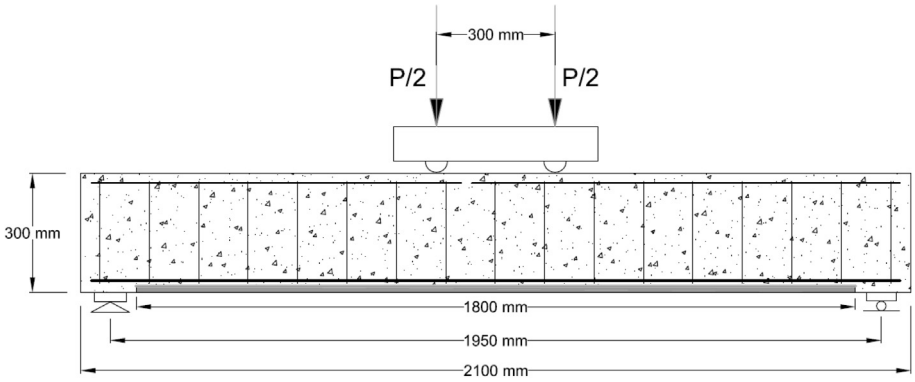

(a)

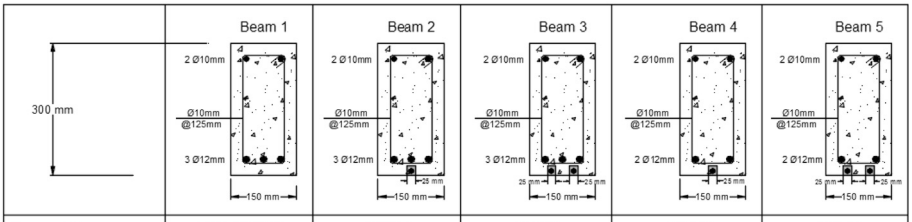

Beam ID	REF-S3B0	S3B1	S3B2	S2B1	S2B2
No. of steel bars	3	3	3	2	2
No. of BFRP bars	0	1	2	1	2

(b)

Fig. 2. (a) Longitudinal section, and (b) cross section detailing of control and strengthened beams.

2.3. Test set-up and instrumentation

The beam specimens were subjected to four-point bending loading with a load span of 0.3 m. Tests were conducted by a 165-kN MTS® servo hydraulic actuator. A steel spreader beam was attached to the actuator to distribute the total load on the two points of loading. Tests were performed in displacement-controlled mode with loading rate of 2 mm/min. The applied loads were recorded by the MTS data acquisition system, while mid-span displacements and strains in concrete surface in the constant moment area were captured using DIC system. Reference image of the undeformed beam was captured prior to loading, to be compared with subsequent images of the deformed beam captured during loading. The images were captured by a single camera with 12 mm lens and 2448 × 2048-pixel resolution. The frame rate of the camera was one frame per second. In order to enable the measurements with the DIC system, a non-periodic high-contrast speckle surface pattern of black dots on white background was applied on the ROI of the beams. In this study, the ROI of the beams was the central 600 × 300 mm region as shown in Fig. 3. Moreover, strain gauges were attached to the BFRP bars to record strains during loading. Fig. 3 shows the test frame with concrete beam specimen and test instrumentation.

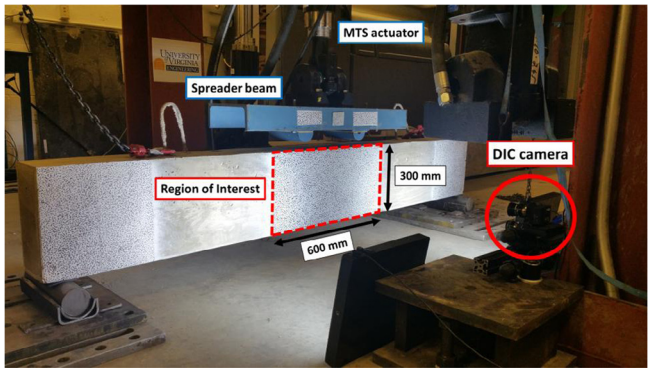

Fig. 3. Four-point bending test setup.

3. Results and discussions

3.1. Flexural behavior of tested RC beams

Fig. 4 shows total load versus mid-span deflection curves of tested RC beams under monotonic loading. The curves started with linear elastic behavior, and all the beams approximately followed the same loading path. The concrete section was not yet cracked and the beams global behavior depended on the gross section properties of the non-cracked concrete. For strengthened beams, bond between BFRP bars, bonding epoxy and concrete was still perfect in that stage. The curves then reached the concrete cracking point, as tension in the concrete bottom fibers at the maximum bending moment zone exceeded the tensile strength of concrete. However, cracks did not occur in the bonding epoxy at this point due to its lower modulus of elasticity compared to concrete, which led to smaller stresses at this deformation level. With increased loading, cracks further propagated in the concrete section, cracks width increased, and new flexural cracks were developed. The force-displacement curves of the beams followed different loading paths, as the global behavior in this stage depended on the amount of steel reinforcement and strengthening BFRP bars, in addition to the properties of the non-cracked portion of the concrete section. The beams then experienced yielding of steel reinforcement, where

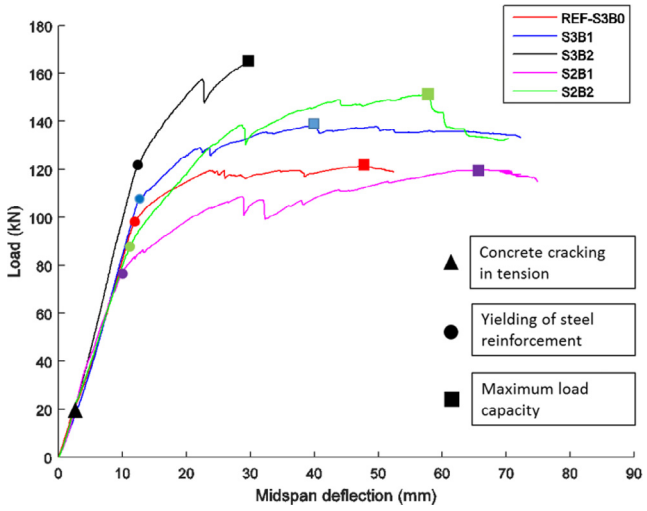

Fig. 4. Total load versus mid-span deflection of tested beams under monotonic loading.

cracks started to develop in the bonding epoxy, and slope of the loading curves started to change. After yielding of steel, the strengthening reinforcement controlled the increase in crack widths. Under continuous loading, cracks continued to propagate in concrete and the bonding epoxy until the top fibers of concrete were crushed in compression. Concrete crushing can be attributed to the increase in the compression stresses at the top of the beam due to propagation of cracks in the compression area. At that point, a small decrease in the load capacity of the beams was observed due to the concrete crushing. However, failure did not occur at this point and all the beams were able to restore their load capacities. The beams were still able to sustain an approximately constant load with significant increase in the deflection until reaching the maximum load capacity. Inclined shear cracks were also observed in the beams, and some of the shear cracks merged or continued as flexural cracks under increased loading. The loading then continued without increase in the load capacity until failure.

Table 1 summarizes test results of all the beams including cracking load (P_{cr}), steel yielding load (P_{sy}) and corresponding moment (M_{sy}), maximum load (P_{max}) and corresponding maximum moment (M_{max}), and mid-span deflection at maximum load (Δ_{Pmax}). Fig. 5(a) shows load versus mid-span deflection curves of test specimens that have three steel bars as the main reinforcement. The inner plot of the figure shows that initial stiffness of strengthened beams were slightly lower than the reference beam until reaching the cracking load. This can be attributed to the fact that the concrete removed from the beam to form the grooves had larger modulus of elasticity than the materials that filled the grooves. While the area of the replaced concrete for one groove was 625 mm^2, the equivalent concrete area of a strengthening bar and filling epoxy, calculated using the transformed section approach, was 178.6 mm^2.

After concrete cracking occurred at about the same load for the three beams, the reference and S3B1 beam had similar stiffness until steel yielding, while the S3B2 beam showed higher stiffness due to larger strengthening reinforcement ratio of that beam. The load at steel yielding and the maximum load for the reference beam were 97.2 kN and 121.3 kN, respectively. The beam specimen strengthened with one BFRP bar (S3B1) exhibited a 9.5% increase in

Table 1
Summary of four-point bending tests results.

Beam	P_{cr} (kN)	P_{sy} (kN)	M_{sy} (kN.m)	P_{max} (kN)	M_{max} (kN.m)	Δ_{Pmax} (mm)
REF-S3B0	20.8	97.2	80.2	121.3	100.1	48.1
S3B1	21.9	106.4	87.8	138.6	114.4	40.0
S3B2*	22.1	122.7	101.2	164.5*	135.7*	29.5*
S2B1	19.3	75.7	62.5	119.7	98.8	65.5
S2B2	21.3	85.1	70.2	151.3	124.8	57.6

* Beam S3B2 did not reach failure because of the actuator capacity.

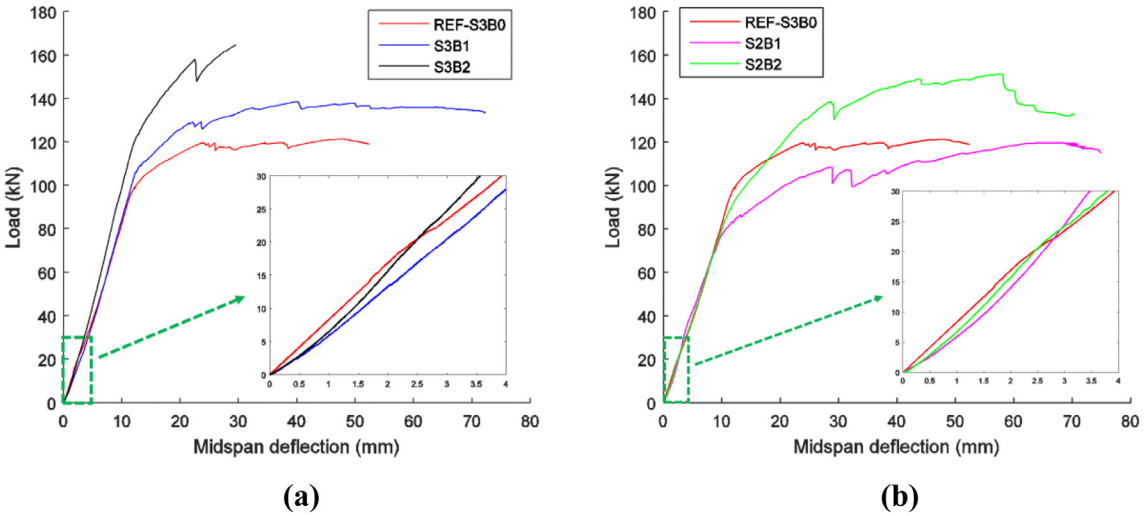

Fig. 5. Total load versus mid-span deflection of (a) REF, S3B1, and S3B2 beams; and (b) REF, S2B1, and S2B2 beams.

the steel yielding load and a 14.3% increase in the maximum load. The deflection at maximum load was 48.1 mm for the reference beam and 40.0 mm for the S3B1 specimen, indicating a 16.8% decrease for the strengthened beam. When two BFRP bars were used for strengthening, the steel yielding load increased by 26.2% to 122.7 kN compared to the reference beam. However, this beam did not reach failure load due to the limited capacity of the actuator. When the test was stopped, the load on the S3B2 specimen was 164.5 kN, suggesting a 35.6% increase compared to the maximum load capacity of the reference beam.

Fig. 5(b) compares the load versus mid-span deflection curves of the reference (S3B0), S2B1 and S2B2 beams. Assuming one of three longitudinal bars in the reference beam was corroded, the S2B1 and S2B2 specimens were designed with only two longitudinal steel bars and were strengthened with BFRP bars in order to restore the flexural capacity. The inner plot of Fig. 5(b) shows that the reference beam exhibited higher stiffness until cracking load. Then, the stiffness of the strengthened beams (S2B1 and S2B2) were almost the same with the reference beam until the steel yielding point was reached. Compared to the reference beam, the steel yielding load of S2B1 and S2B2 specimens decreased by 22.1%, and 12.5%, respectively due to the lower amount of steel reinforcement and lower modulus of elasticity of BFRP bars. However, the S2B1 beam was able to reach 98.7% of the maximum load capacity of the reference beam, with a 36.2% increase in the maximum deflection compared to the reference beam. In addition, the maximum load capacity and the corresponding deflection of the S2B2 beam increased by 24.7% and 19.8%, respectively compared to the reference beam. Note that the deflection at the maximum load for the beam strengthened with two BFRP bars (S2B2) was lower than that of the beam strengthened with one BFRP bar (S2B1) due to the increasing strengthening reinforcement ratio. Nevertheless, both strengthened beams exhibited higher deflection capacity than the reference beam. This could be attributed to the lower modulus of elasticity of BFRP bars compared to steel reinforcement. These results suggest that NSM BFRP bars can effectively restore or even increase the load carrying capacity of the RC beams with corroded tensile longitudinal bars while providing a more ductile response.

In strengthened beams, strain gauges were attached to the BFRP bars at mid-span to monitor tensile strains in the bars during loading. Fig. 6 shows the total load-strain curves of strengthened beams categorized in two groups. It can be seen that the points of concrete cracking, and steel yielding can be distinguished, where changes in the slope of the curves were observed. As shown in Fig. 6(a), the strain in the BFRP bar of S3B1 beam remained very low until reaching 0.05% at the cracking load of 15.6 kN. Afterwards, the strain in the bar increased linearly with a higher rate up to 0.36% at the steel yielding load of 89.4 kN. A nonlinear and significant increase in the strain of the BFRP bar was observed until reaching the maximum load capacity, where the strain was 2.12%. This strain value was 66% of the ultimate strain capacity of the BFRP bars. It should be noted that there is a slight difference between the values of concrete cracking and steel yielding loads previously obtained from load-deflection curves and those loads obtained from load-strain curves. This can be attributed to the different nature of measurements (i.e. distributed versus pointwise measurements) captured by the DIC and strain gauges. The strain data obtained from the strengthening bar of the S3B2 beam showed similar behavior with that of the S3B1 specimen. The load-strain curve of the beam reached the concrete cracking point at a strain of 0.06% and steel yielding at 0.35% strain. However, the attached strain gauge was damaged at a load of 113.4 kN at 0.75% strain and no further data was obtained.

Fig. 6(b) shows the load-strain curves for the S2B1 and S2B2 specimens. No concrete cracking point was detected from the load-strain curve of the S2B1 beam, while the concrete cracking load of the S2B2 beam was 25.1 kN that occurred when the strain in the BFRP bar was 0.07%. At the steel yielding point, the strain in the BFRP bar was 0.25% for the S2B1 specimen and 0.35% for the S2B2 specimen. The strain gauge in the S2B1 beam recorded the data until it was damaged at a load of 103.7 kN and strain of 1.29%. The strain in the BFRP bar of the S2B2 beam was 2.27% when the beam reached its maximum load capacity. This strain was about 71% of the average ultimate strain of the BFRP bars.

3.2. Cracks width measurement and failure modes

The distribution of major principal strain was plotted over the ROI of each beam using the DIC to assess the distribution of cracks on beams surface and enable measurements of cracks width. Fig. 7 shows contours of principle longitudinal strain of tested beams at steel yielding load, load at which the concrete top fibers were crushed and parts of the top concrete were split (P_c), and the maximum load. Relatively small cracks were identified on the contours map where a significant increase in the strain was observed,

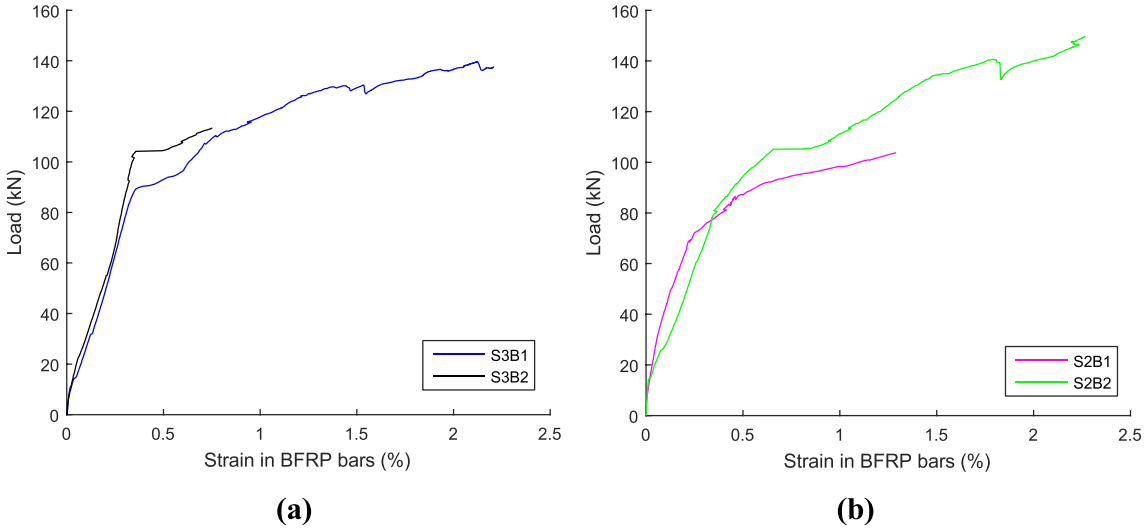

Fig. 6. Total load versus strains in BFRP bars for (a) S3B1 and S3B2 beams; and (b) S2B1 and S2B2 beams.

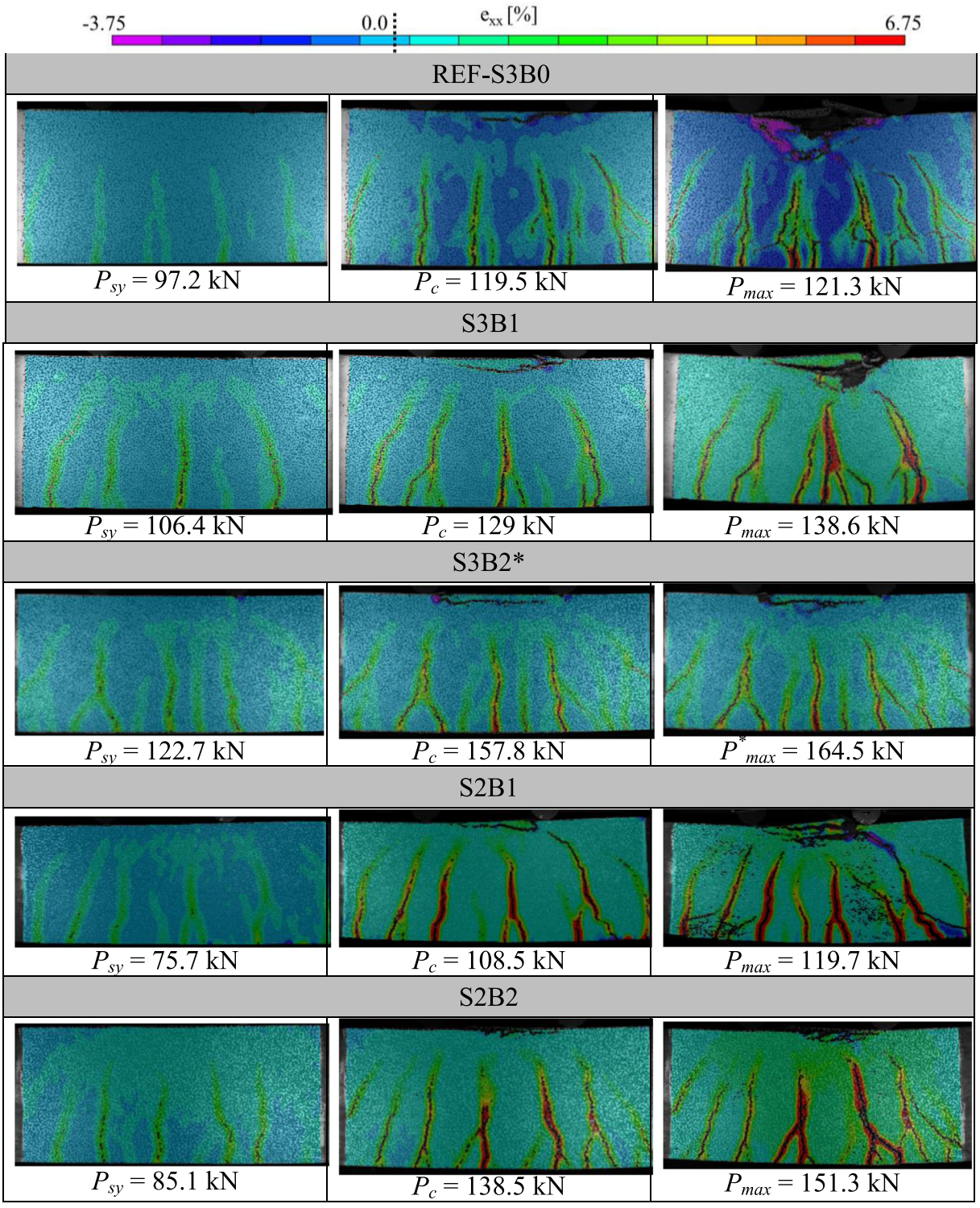

Fig. 7. Distribution of principle longitudinal strains on tested beams at different loading stages (*Beam S3B2 did not reach failure because of the actuator capacity).

whereas large cracks were identified as a discontinuity in the strain map. It can be seen that all strengthened beams, except the S2B1 beam, showed more localized crack distribution in the maximum moment zone and less degree of concrete crushing in the compression area compared with reference beam.

The longitudinal component of the displacement field was also measured on a horizontal line at the main reinforcement level and plotted for each beam as shown in Fig. 8. The sudden jumps in the horizontal displacement plots were due to the crack openings, and a crack width can be measured as the magnitude of the relevant jump. Horizontal displacements were plotted at loads of concrete cracking, steel yielding, top concrete crushing, and maximum load capacity of each beam to show the evolution of cracks width under continuous loading. In all the beams, the horizontal displacements were relatively small at the concrete cracking and steel yielding stages, and significantly increased afterwards until reaching the

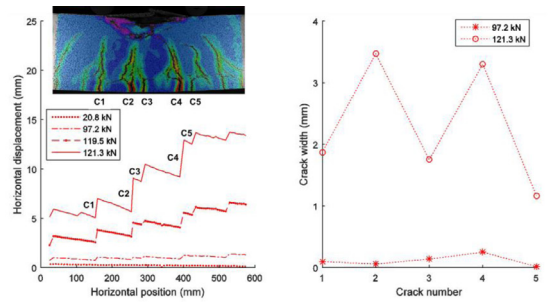

(a) REF-S3B0

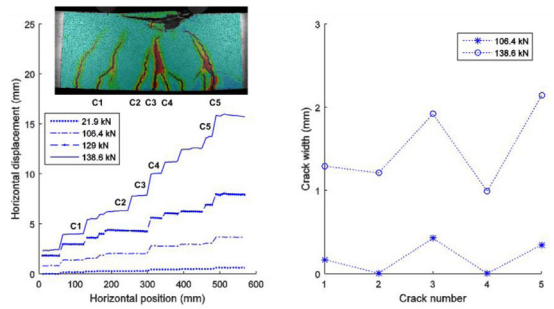

(b) S3B1

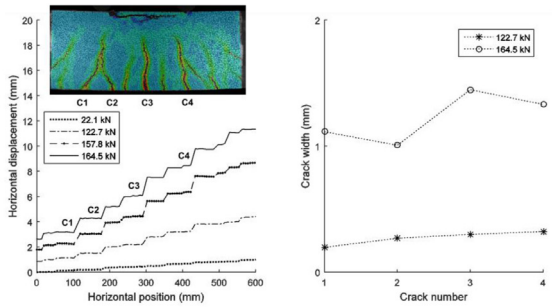

(c) S3B2

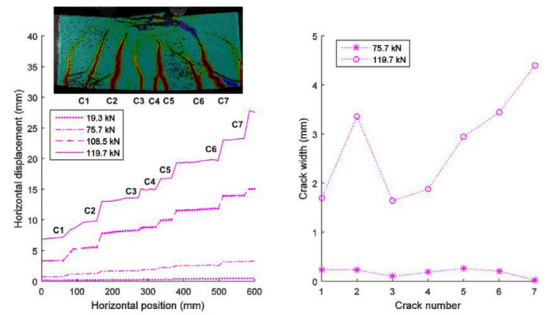

(d) S2B1

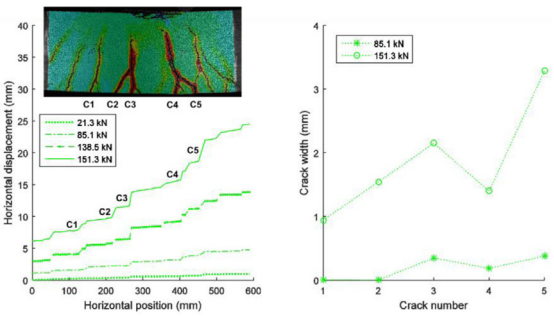

(e) S2B2

Fig. 8. Horizontal displacement plotted at main reinforcement level versus horizontal position, and width of major cracks in tested beams: (a) REF; (b) S3B1; (c) S3B2; (d) S2B1; and (e) S2B2 beam.

maximum capacity. This is a result of the higher rate of increase in the cracks openings after yielding of main steel reinforcement. Fig. 8 also shows the numbering of major cracks in each beam and plots the corresponding crack widths at steel yielding load and maximum capacity. Among the beams with three steel reinforcing bars, the reference beam obtained relatively smaller cracks than the S3B1 and S3B2 specimens at the steel yielding stage. However, at its maximum load of 121.3 kN, the reference beam experienced higher number of large cracks with a maximum crack width of 3.47 mm. The strengthened beams obtained lower maximum crack widths of 2.14 mm at maximum load of 138.6 kN for the S3B1 beam, and of 1.45 mm at maximum load of 164.5 kN in the S3B2 beam. This can be attributed to the effect of strengthening reinforcement in controlling the cracks widths after yielding of main reinforcement.

As can be seen from Fig. 8(d), in comparison with the reference beam, the S2B1 specimen obtained wider cracks with a maximum crack width of 4.39 mm at a maximum load of 119.7 kN. Note that the S2B1 specimen sustained larger deflections than the reference beam. Using two strengthening bars enabled better control of crack width after yielding of steel. The S2B2 beam obtained a lower crack width of 3.29 mm at its maximum load of 151.3 kN compared to the S2B1 beam. This maximum crack width for the S2B2 beam was also slightly lower than the maximum crack width of the reference beam, although the maximum load and deflection of the S2B2 was higher.

Fig. 9 shows the failure modes of the tested RC beams. In the reference beam, flexural cracks were first formed and then the top fibers of concrete were crushed. Under continuous loading, the cracks further propagated in the compression zone, and additional concrete crushing occurred until reaching the point of complete failure. Some minor shear cracks were also observed in the beam, but the shear cracks were not the cause of beam failure. Failure of the reference beam was ductile gradual flexural failure. The S3B1 beam followed the same flexural behavior of the reference beam and experienced similar mode of failure. Due to the higher deflection capacity in comparison with the reference beam, the S3B1 beam experienced wider and larger number of cracks at complete failure. However, at maximum load, the width of the largest crack in the S3B1 beam was still smaller than the largest crack in the reference beam. The S3B2 beam did not reach complete failure due to the actuator capacity, therefore, relatively small flexural cracks and minor concrete crushing were observed in the specimen. The S2B1 beam experienced flexural cracks at the concrete cracking stage and reached to the crushing of the compression zone under continues loading. The beam also experienced relatively large combined shear and flexure crack in the area of combined maximum moment and shear. However, the beam failed in ductile flexural mode. The S3B2 beam experienced different mode of failure compared with the other beams. The individual flexural cracks were first observed in the beam. Those cracks were then merged together to form wider cracks under further loading. At failure, sudden and complete separation of the bottom concrete cover occurred in the beam, with much lesser degree of concrete crushing compared to the other beams. In all the beams, no rupture was observed in the strengthening BFRP bars.

4. Conclusions

A total of five concrete beams with different internal steel reinforcement ratio were fabricated. The beams were strengthened with different ratios of basalt FRP bars using NSM technique and tested in four-point bending under monotonic loading. DIC system was used to perform full-field strain and displacement

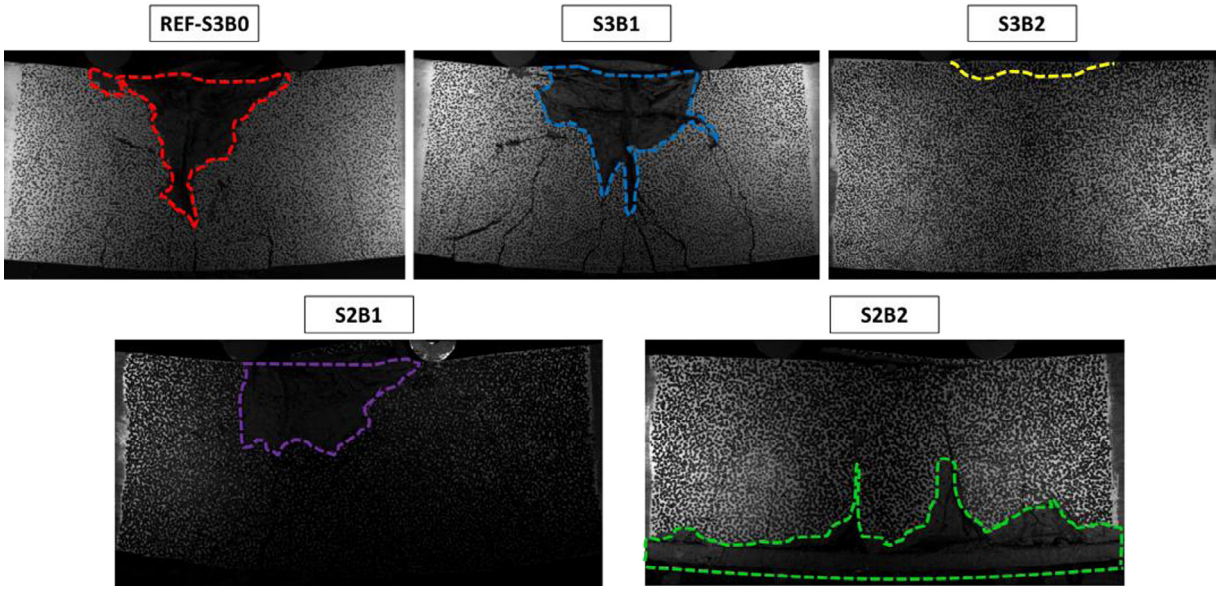

Fig. 9. Modes of failure of concrete beams tested in four-point bending.

measurements on the constant moment zone in each beam. These measurements were used to calculate mid-span deflection, plot distribution of principle strains, and monitor crack propagation. The strain gauges were also attached to the BFRP bars to calculate tensile strains during loading. The findings of this study can be summarized as follows:

- When an RC beam with three internal steel reinforcement was strengthened with one or two NSM BFRP bars, the maximum load capacity increased by 14.3% and 35.6%. However, note that the test was stopped due to the limited actuator force capacity for the beam strengthened with two BFRP bars. For the beam strengthened with one BFRP bar, the maximum deflection decreased 16.8%.
- The largest crack width at the maximum load was 3.47 mm for the reference beam, while it was 2.14 mm and 1.45 mm for the beam strengthened with one or two BFRP bars, respectively.
- Assuming one of three steel bars was corroded, using one BFRP bar restored the load capacity of the concrete beam and provided 36.2% higher deflection capacity, indicating more ductile behavior compared to the intact beam. Using two BFRP bars to strengthen the same beam, increased the load capacity by 24.7% compared to the reference beam and provided 19.8% higher deflection and slightly smaller cracks at the maximum load.
- The beams strengthened with one BFRP bars exhibited a ductile flexural failure mode. Increasing the strengthening reinforcement resulted in more brittle behavior.
- The strain in BFRP bars recorded at the maximum load in the strengthened beams was about 71% of the ultimate strain of the BFRP bars, suggesting a high strength utilization ratio for the NSM reinforcement.

Results of this study indicate that BFRP bars can be environmentally-friendly and cost-effective option for NSM strengthening applications.

Acknowledgements

The authors would like to acknowledge the support of Center for Infrastructure Renewal and Advanced Materials at University of Virginia to conduct this research. The authors would also like to thank Neuvokas, Inc. for providing the BFRP bars at no cost.

References

[1] Huang RY, Mao I, Lee HK. Exploring the deterioration factors of RC bridge decks: a rough set approach. Comput Aid Civ Infrastruct Eng 2010;25(7):517–29.
[2] Teng JG, Chen JF, Smith ST, Lam L. FRP strengthened RC structures. U.K.: John Wiley & Sons Publishing; 2002.
[3] Bakis C, Bank LC, Brown V, Cosenza E, Davalos JF, Lesko JJ, et al. Fiber-reinforced polymer composites for construction-state-of-the-art review. J Compos Constr 2002;6(2):73–87.
[4] Hollaway LC, Teng JG. Strengthening and rehabilitation of civil infrastructures using fibre-reinforced polymer (FRP) composites. Cambridge, U.K.: Woodhead Publishing; 2008.
[5] Lorenzis LD, Nanni A. Characterization of FRP rods as near-surface mounted reinforcement. J Compos Constr 2001;5(2):114–21.
[6] El-Hacha R, Rizkalla SH. Near-surface-mounted fiber-reinforced polymer reinforcements for flexural strengthening of concrete structures. ACI Struct J 2004;101(5):717–26.
[7] Oudah F, El-Hacha R. Fatigue behavior of RC beams strengthened with prestressed NSM CFRP rods. Compos Struct 2012;94(4):1333–42.
[8] Kotynia R. Bond between FRP and concrete in reinforced concrete beams strengthened with near surface mounted and externally bonded reinforcement. Constr Build Mater 2012;32:41–54.
[9] Seracino R, Raizal Saifulnaz MR, Oehlers DJ. Generic debonding resistance of EB and NSM plate-to-concrete joints. J Compos Constr 2007;11(1):62–70.
[10] Bonacci JF, Maalej M. Behavioral trends of RC beams strengthened with externally bonded FRP. J Compos Constr 2001;5(2):102–13.
[11] Ceroni F, Pecce M, Bilotta A, Nigro E. Bond behavior of FRP NSM systems in concrete elements. Compos B Eng 2012;43(2):99–109.
[12] Sharaky IA, Torres L, Baena M, Vilanova I. Effect of different material and construction details on the bond behaviour of NSM FRP bars in concrete. Constr Build Mater 2013;38:890–902.
[13] Seo SY, Feo L, Hui D. Bond strength of near surface-mounted FRP plate for retrofit of concrete structures. Compos Struct 2013;95:719–27.
[14] Bilotta A, Ceroni F, Di Ludovico M, Nigro E, Pecce M, Manfredi G. Bond efficiency of EBR and NSM FRP systems for strengthening concrete members. J Compos Constr 2011;15(5):757–72.
[15] Barros JA, Fortes AS. Flexural strengthening of concrete beams with CFRP laminates bonded into slits. Cem Concr Compos 2005;27(4):471–80.
[16] Capozucca R. Static and dynamic response of damaged RC beams strengthened with NSM CFRP rods. Compos Struct 2009;91(3):237–48.
[17] Al-Mahmoud F, Castel A, François R, Tourneur C. RC beams strengthened with NSM CFRP rods and modeling of peeling-off failure. Compos Struct 2010;92(8):1920–30.
[18] Sharaky IA, Torres L, Comas J, Barris C. Flexural response of reinforced concrete (RC) beams strengthened with near surface mounted (NSM) fibre reinforced polymer (FRP) bars. Compos Struct 2014;109:8–22.
[19] El-Gamal SE, Al-Nuaimi A, Al-Saidy A, Al-Lawati A. Flexural strengthening of RC beams using near surface mounted fibre reinforced polymers. In:

Engineering and technology (BICET 2014), 5th Brunei international conference. IET. p. 1–7.
[20] Dhand V, Mittal G, Rhee KY, Park SJ, Hui D. A short review on basalt fiber reinforced polymer composites. Compos B Eng 2015;73:166–80.
[21] El Refai A. Durability and fatigue of basalt fiber-reinforced polymer bars gripped with steel wedge anchors. J Compos Constr 2013;17(6):04013006.
[22] Sim J, Park C. Characteristics of basalt fiber as a strengthening material for concrete structures. Compos B Eng 2005;36(6):504–12.
[23] Manikandan V, Jappes JW, Kumar SS, Amuthakkannan P. Investigation of the effect of surface modifications on the mechanical properties of basalt fibre reinforced polymer composites. Compos B Eng 2012;43(2):812–8.
[24] Wang X, Shi J, Liu J, Yang L, Wu Z. Creep behavior of basalt fiber reinforced polymer tendons for prestressing application. Mater Des 2014;59:558–64.
[25] Zhu H, Wu G, Zhang L, Zhang J, Hui D. Experimental study on the fire resistance of RC beams strengthened with near-surface-mounted high-Tg BFRP bars. Compos B Eng 2014;60:680–7.
[26] Gopinath S, Murthy AR, Patrawala H. Near surface mounted strengthening of RC beams using basalt fiber reinforced polymer bars. Constr Build Mater 2016;111:1–8.
[27] Shih MH, Sung WP. Application of digital image correlation method for analysing crack variation of reinforced concrete beams. Sadhana 2013;38 (4):723–41.
[28] Gencturk B, Hossain K, Kapadia A, Labib E, Mo YL. Use of digital image correlation technique in full-scale testing of prestressed concrete structures. Measurement 2014;47:505–15.
[29] Mahal M, Blanksvärd T, Täljsten B, Sas G. Using digital image correlation to evaluate fatigue behavior of strengthened reinforced concrete beams. Eng Struct 2015;105:277–88.
[30] Shah SG, Kishen JC. Fracture properties of concrete–concrete interfaces using digital image correlation. Exp Mech 2011;51(3):303–13.
[31] Carloni C, Subramaniam KV, Savoia M, Mazzotti C. Experimental determination of FRP–concrete cohesive interface properties under fatigue loading. Compos Struct 2012;94(4):1288–96.
[32] Nonis C, Niezrecki C, Yu TY, Ahmed S, Su CF, Schmidt T. Structural health monitoring of bridges using digital image correlation. In: SPIE smart structures and materials + nondestructive evaluation and health monitoring. International Society for Optics and Photonics; 2013.